# $^{12}$C($^{16}$O,$\gamma$)$^{28}$Si radiative capture: Structural and statistical aspects of the $\gamma$ decay

D. Lebhertz,[1,2] S. Courtin,[1,*] F. Haas,[1,†] D. G. Jenkins,[3] C. Simenel,[4] M.-D. Salsac,[1,4] D. A. Hutcheon,[5] C. Beck,[1] J. Cseh,[6]
J. Darai,[7] C. Davis,[5] R. G. Glover,[3] A. Goasduff,[1] P. E. Kent,[3] G. Levai,[6] P. L. Marley,[3] A. Michalon,[1] J. E. Pearson,[5]
M. Rousseau,[1] N. Rowley,[8] and C. Ruiz[5]

[1]*Université de Strasbourg, IPHC, 23 rue du Loess, 67037 Strasbourg, France, and CNRS, UMR7178, 67037 Strasbourg, France*
[2]*GANIL, CEA-DSM, and CNRS-IN2P3, Caen, France*
[3]*University of York, York, United Kingdom*
[4]*CEA, Centre de Saclay, IRFU/Service de Physique Nucléaire, Gif sur Yvette, France*
[5]*TRIUMF, Vancouver, Bristish Columbia, Canada*
[6]*Institute of Nuclear Research of the Hungarian Academy of Sciences, Debrecen, Hungary*
[7]*Institute of Experimental Physics, University of Debrecen, Debrecen, Hungary*
[8]*IPNO, Université de Paris Sud, CNRS-IN2P3, Paris, France*

The heavy-ion radiative capture reaction $^{12}$C($^{16}$O,$\gamma$)$^{28}$Si has been studied at three energies $E_{\text{c.m.}} = 8.5$, 8.8, and 9 MeV which are close to the Coulomb barrier. The weak radiative capture process has been identified by measuring the $^{28}$Si recoils in the highly selective 0° spectrometer DRAGON at TRIUMF (Vancouver). The coincident $\gamma$ rays have been recorded in the associated BGO array. This has allowed a complete measurement of the $\gamma$ spectrum and the relative strength of all decay pathways. An important part of the decay through quasibound states close to the particle threshold and the feeding of bound states with particular deformation have been identified for the first time. Comparisons with Monte Carlo simulations allowed the extraction of the full experimental radiative capture cross section. Our results suggest an important contribution of spins $J^\pi = 5^-$ and $6^+$ in the entrance channel. The surprisingly large cross sections from 12 $\mu$b at $E_{\text{c.m.}} = 8.5$ MeV to 25 $\mu$b at $E_{\text{c.m.}} = 9.0$ MeV for the heavy-ion radiative capture process are discussed in terms of the interplay between statistical and structural aspects of the process.

## I. INTRODUCTION

Clustering is a highly collective phenomenon which can occur at different scales of the physical world from astrophysical down to the subatomic level. For instance, galaxies evolving in clusters are held together by gravity and atoms can form robust systems of sizes larger than molecules, called fullerenes. Inside nuclear matter, clustering has been observed in several *p*-shell nuclei (Be, Li, $^{12-14}$C, and $^{16}$O) [1]. For these nuclei, the elementary substructure is the very stable $\alpha$ particle whose binding energy is large and the energy of its first excited state is 20.21 MeV. Numerous theoretical calculations reproduce the energies and spectroscopic properties of these states; they also predict new states built on heavier substructures for nuclei in the *sd* shell. Whereas the $\alpha$ particle is known to be the most important substructure for light nuclei, $^{12}$C is expected to play the same role for *sd*-shell nuclei. Such a cluster structure is thus expected in $^{24}$Mg($^{12}$C-$^{12}$C) and $^{28}$Si($^{12}$C-$^{16}$O). Concerning $^{28}$Si, recent cluster calculations predict the emergence of such bands at different excitation energies with bound, quasibound or molecular structure [2–5]. A possible unified description of $^{28}$Si in terms of $^{24}$Mg + $\alpha$ and $^{12}$C + $^{16}$O clustering has already been discussed some time ago in Ref. [6]. Cluster bands are obtained with $^{24}$Mg + $\alpha$ substructure for the oblate ground-state (g.s.) band and for a quasibound band starting at higher excitation energy in

$^{28}$Si. Three prolate deformed bands with, at least partially, $^{12}$C-$^{16}$O structure are also found: the first band is bound and corresponds well to the $^{28}$Si known prolate band, starting at $E(0_3^+) = 6.69$ MeV, the second one is an unknown quasibound band, and the third band is a resonant one. This third band could explain the occurrence of the known narrow resonances in $^{12}$C + $^{16}$O which happen around the Coulomb barrier (CB) ($E_{\text{CB}} \sim 7.9$ MeV) and which are correlated in several fusion channels [7–9]. This band is predicted to start close to the CB and could also be related to the $^{12}$C-$^{16}$O breakup band measured in $^{28}$Si by the CHARISSA Collaboration [10]. In that work, the breakup of $^{28}$Si into $^{12}$C + $^{16}$O has been studied at excitation energies $E^*$ in $^{28}$Si ranging from 28 to 50 MeV via the $^{12}$C($^{20}$Ne,$^{12}$C$^{16}$O)$\alpha$ reaction. By measuring fragment-fragment angular correlations, the authors were able to deduce the spins of these breakup states. The corresponding spin systematics shows that the breakup states form a band with large moment of inertia, typically the same as for a highly deformed molecular structure. The bandhead and low-lying members of the breakup band should lie close to the CB, i.e., in the same $^{28}$Si excitation energy region covered in our experiment. A complete understanding of the occurrence of the resonances at and below the CB in collisions between light heavy ions is important since such resonances, particularly strong in $^{12}$C + $^{12}$C, have been found in this system down to energies close to the Gamow window [11]. This has major consequences in extrapolating cross-section results down to the astrophysical energy region. Even if $^{24}$Mg states based on $^{12}$C substructures are predicted by microscopic [12] and semimicroscopic [13] cluster calculations in this energy range,

─────────
*sandrine.courtin@iphc.cnrs.fr
†florent.haas@iphc.cnrs.fr

a clear $\gamma$-decay signature is still needed. The radiative capture (RC) process, which is the exclusive $\gamma$-decay part of the fusion process, is a good tool to probe at the same time the overlap between the entrance channel and states of the composite system, as well as the overlap between these states. For this reason, we have started a campaign of experiments in the $^{12}C + ^{12}C$ and $^{12}C + ^{16}O$ systems in order to identify the complete $\gamma$-decay scheme of the RC process.

The $^{12}C(^{12}C,\gamma)^{24}Mg$ heavy-ion RC was investigated close to the CB at the beginning of the 1980s [14]. Significant capture cross sections and narrow resonances in the partial decay cross sections through low-lying states were identified. To investigate the origin of this phenomena, three new experiments have been performed to measure the total RC cross section and the complete $\gamma$-decay pattern. The first experiment was performed with the Argonne Fragment Mass Analyzer (FMA), and the second with Gammasphere in Berkeley used in a calorimeter mode. Both experiments showed that part of the $\gamma$ flux is mediated through medium excitation energy states in $^{24}Mg$ [15]. In order to measure with high statistics the complete $\gamma$ decay of the RC, an experiment with similar setup to the one discussed in the present article was performed at TRIUMF (Vancouver) using DRAGON and its associated BGO array. The improvement of this experiment is that it enables selection of the RC recoil nuclei to get access to the full $\gamma$-decay pattern. This experiment shows that more than 50% of the $\gamma$ flux is going through doorway states around 10 MeV in the compound $^{24}Mg$ nucleus [16].

The $^{12}C(^{16}O,\gamma)^{28}Si$ heavy-ion RC reaction was also investigated close to the CB [14]. Similar to the $^{12}C + ^{12}C$ case, significant capture cross sections and narrow resonances in the partial cross sections through low-lying states have been identified. The phenomenon was then probed deeper by coupling the previously used large NaI $\gamma$ detector with a Wien filter device to partially select the recoil nuclei [17], allowing the observation for the first time of a 2-$\mu$b cross section through states around 7 MeV in $^{28}Si$. This was interpreted by the authors in terms of the feeding of the $0^+$ and $2^+$ states of the prolate rotational band.

To validate the hypothesis of the molecular origin of the resonant phenomena and to locate eventual intermediate excitation energy states with a $^{12}C$-$^{16}O$ substructure, it is of interest to find the $\gamma$ link between the resonant band and the lower energy bands predicted. Measurement of the complete $\gamma$-decay pattern of the RC reaction is a unique way to probe the link between resonant cluster structure and bound or quasibound states. A resonance based on a molecular structure of the composite nucleus should exhibit enhanced $E2$ electromagnetic transitions to similarly deformed lower-lying states with $^{12}C$-$^{16}O$ substructure. As the setup is identical to the one used for the $^{12}C(^{12}C,\gamma)^{24}Mg$ experiment, this new set of data is complementary and provides the advantage of probing the $^{28}Si$ microlaboratory, where oblate, prolate, and octupole shapes coexist [18]. Indeed, in this nucleus, the $^{12}C$-$^{16}O$ configuration has a weak overlap with the oblate g.s. band and a strong overlap with the prolate band, with both bands lying at relatively low excitation energy. The relative strength of all the decay paths of the RC can highlight in this system a cleaner view of the mechanism and structure effects
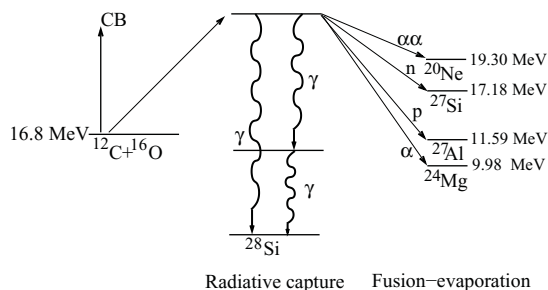


FIG. 1. Schematic view of the possible exit channels of the $^{12}C + ^{16}O$ reaction. The threshold energies of the different channels are given with reference to the $^{28}Si$ ground state.

involved. In this article, we propose to discuss the structural and statistical aspects of the RC $\gamma$ decay in this particular microlaboratory.

## II. $^{12}C(^{16}O,\gamma)^{28}SI$ EXPERIMENT AT TRIUMF

### A. Choice of the DRAGON-BGO apparatus

In the previous Sandorfi *et al.* $^{12}C(^{16}O,\gamma)^{28}Si$ RC study, strong resonant structures were found in the decay to the $^{28}Si$ ground state and to the first excited state [14,17], between $E_{c.m.} = 6.5$ and 12 MeV. We have chosen to revisit this reaction at two energies corresponding to maxima of the excitation function—at $E_{c.m.} = 8.5$ and 9 MeV—and to a minimum at $E_{c.m.} = 8.8$ MeV. These three bombarding energies correspond to excitation energies of the $^{28}Si$ CN of 25.3, 25.8, and 25.6 MeV, respectively. The aim of the experiment was to measure for the first time the full decay spectrum of the $^{12}C(^{16}O,\gamma)^{28}Si$ reaction making use of the DRAGON 0° spectrometer to select the $^{28}Si$ recoils at the focal plane. From an experimental point of view, such a measurement is very challenging due to the competition with fusion-evaporation channels. At the $^{12}C + ^{16}O$ CB, a $^{28}Si$ excitation energy region around 25 MeV is reached. At this energy, $\alpha$, $p$, and $n$ channels are open, as indicated in Fig. 1, and dominate the deexcitation process. The ratio between the fusion cross section and the RC cross section is expected to be around $10^5$, with fusion thus giving rise to the main part of the direct $\gamma$ spectrum. This explains why the previous experiments [14,17] did not have access to the complete $\gamma$ spectrum and thus only measured the decay to the low-lying states of $^{28}Si$. In this study, we have chosen to select the RC channel by measuring the compound nucleus recoils at 0° and to record the coincident $\gamma$ rays in a BGO scintillator $\gamma$ array. To achieve this, a $\gamma$ detector of high efficiency for $\gamma$ energies between 1 and 25 MeV is needed, as well as a very efficient selection of the recoil nuclei around 0°, i.e., with a beam rejection factor better than $10^{12}$. These requirements were fulfilled by the DRAGON spectrometer and its BGO array [19] situated at the TRIUMF Laboratory in Vancouver (Canada). The setup has been designed for 0° RC experiments on light gas targets in inverse kinematics; the acceptance of the spectrometer is therefore not 100% for our heavy-ion radiative capture experiment. The DRAGON spectrometer has

nevertheless allowed us to get a $10^{13}$ rejection factor of the incident beam and to detect the recoil nuclei in a double-sided silicon strip detector (DSSSD) at the spectrometer focal plane. Details about the setup can be found in Ref. [19]. The BGO array around the target has been designed to be as efficient as possible with 30 detectors in a closed geometry covering 90% of $4\pi$, leading to an efficiency of 30% for 10-MeV $\gamma$ rays.

### B. Experimental details

The experiment was performed at three $^{16}$O beam energies, $E_{\text{Lab}} = 19.8$, 20.5, and 21.0 MeV, with a typical current of 10 pnA. The choice of the bombarding energies is explained in the previous section. Three highly enriched (99.9%) $^{12}$C thin targets of $\sim$40 $\mu$g/cm$^2$ thickness were used. The DRAGON gas-target system was replaced by a system to support solid targets. The relative thickness of the three targets used and the buildup of $^{12}$C during the experiment have been carefully monitored by measuring the total $\gamma$ flux in the BGO array. The thickness of the target has been monitored to ensure on-resonance results and the settings of the DRAGON spectrometer have been optimized accordingly. To limit the counting rate in the BGOs, the threshold of the BGO detectors was set to around 1.2 MeV, in order to be able to record the $^{28}$Si $2_1^+ \rightarrow 0_1^+$ (1.78-MeV) transition. The use of the solid target system allowed the alteration of the beam pipe at the entrance of DRAGON to reach a 25 mrad acceptance of the spectrometer. In our case, the maximum angular spread was 33 mrad, which corresponds to a deviation of the recoils by high-energy $\gamma$ rays of 25 MeV emitted at 90° with respect to the beam axis. The limited acceptance of DRAGON, due to the specific $\gamma$ decay of our reaction, implies to fully understand how the spectrometer filters the $\gamma$ spectrum in coincidence with the recoil nuclei measured in the DSSSD. The specific setup of DRAGON will be presented in the following section. Limitations due to the nature of the $\gamma$ rays emitted show that, to obtain quantitative results, a complete simulation of the BGO array and spectrometer has to be done to perform the data analysis.

### C. Setting up DRAGON

In order to set up DRAGON, the beam is first bent by the first magnetic dipole to get an accurate measurement of the beam energy. Then the different fields are set in order to reach a 100% transmission of the beam down to the Faraday cup in front of the focal plane. A scaling procedure is then used to select $^{28}$Si recoils with charge state $q = 8$. The optimal setup of the optical elements depends on the energy of the recoil nucleus. The DRAGON acceptance as a function of the recoil energy has been estimated by simulations using GEANT3. The results are shown in Fig. 2. The simulation has been performed for two types of decay: a one-step decay to the $^{28}$Si g.s. involving a high-energy $\gamma$ ray and a two-step decay involving two cascade $\gamma$ rays of equal energies. Calculations have been performed in the case of isotropic and $E1$ transitions. The response of the spectrometer is very different and highly sensitive to the $\gamma$-ray emission angle with respect to the beam axis, especially
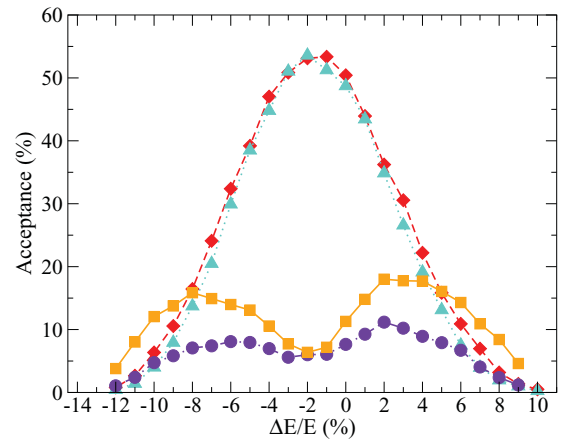


FIG. 2. (Color online) Acceptance of the $^{28}$Si recoils at the DRAGON focal plane as a function of the mistune $\Delta E/E$ around the expected value $E$ of the recoil energy. These calculations have been used for setting up the spectrometer. Results are shown for a decay involving a unique $\gamma$ of 25 MeV emitted isotropically (orange squares) and following an $E1$ distribution (violet circles) and for a cascade of two $\gamma$ rays of 12.5 MeV each, for an isotropic distribution (red diamonds) and following an $E1$ distribution (blue triangles).

for high-energy $\gamma$ rays. As seen in Fig. 2, the maximum of the acceptance curve is at $\Delta E/E \sim -2.5\%$ for the two-step decay and at $-7.5\%$ and $+2.5\%$ for the one-step decay. Since we were mainly interested in measuring the cascade involving intermediate-energy states, the main part of the measurement was performed at $\Delta E/E = -2.5\%$. Results of the numerical simulations have been checked by measuring the transmission for different recoil energies close to the expected one. The maximum acceptance and transmission measured with the target was between $-3\%$ and $-1\%$, in agreement with simulations.

### D. Radiative capture selection

In order to select the RC channel, a gate has been set on the time of flight–$E_{\text{DSSSD}}$ spectrum. The time of flight (TOF) corresponds to the time between the first $\gamma$ ray detected ($\gamma$ trigger) in the BGO and a recoil nucleus detected in the DSSSD (recoil trigger).

This identification spectrum is very clean for the data at 8.5 MeV (see Fig. 3) and 8.8 MeV and the $^{28}$Si region can easily be selected. At $E_{\text{c.m.}} = 9$ MeV, a second component with energy around 11 MeV appears in the $E_{\text{rec}}$ spectrum (Fig. 4, top), which is in coincidence with specific $^{24}$Mg and $^{27}$Al $\gamma$ rays. It could come from a value of $q/A$ common to $^{28}$Si and $^{24}$Mg or $^{28}$Si and $^{27}$Al. In order to minimize effects of this contamination, we have sharpened the selection around the $^{28}$Si peak to maximize the $\gamma$ rate ratio of $E_\gamma > 10$ MeV on $E_\gamma < 10$ MeV. As can be seen in Fig. 4 (bottom), this ratio is a good discriminant since, unlike the RC, the $\gamma$ rays associated with $^{24}$Mg and $^{27}$Al coming from fusion-evaporation channels do not have energies higher than 10 MeV.
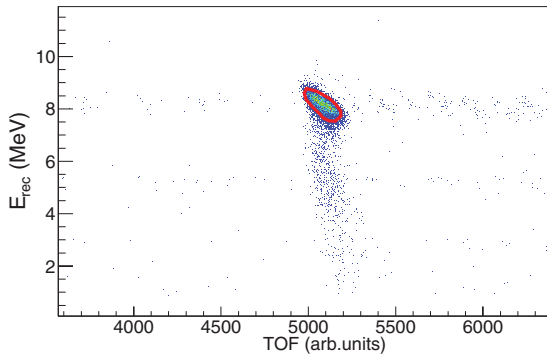
FIG. 3. (Color online) Energy of the recoil nuclei as a function of the TOF between the $\gamma$ ray and the recoil nucleus at $E_{c.m.} = 8.5$ MeV.

## III. RESULTS

### A. General behavior of the $\gamma$ spectrum

After selection of the $^{28}$Si, the $\gamma$ spectra are given in Fig. 5 for the three bombarding energies of this experiment. The three spectra are characterized by a prominent bump at around 14 MeV. The width of this bump is approximately 5 MeV and corresponds to the feeding of at least three states around 11 MeV in $^{28}$Si, slightly above the $\alpha$ threshold at 9.98 MeV. This bump is observed at the three bombarding energies and its intensity does not seem to be correlated with the previously observed resonances in RC decay to low-lying states of $^{28}$Si [14,17]. In the low-energy part of the spectrum we can see $^{28}$Si peaks at 1.78 MeV ($2_1^+ \rightarrow 0_1^+$) and at 2.84 MeV ($4_1^+ \rightarrow 2_1^+$),
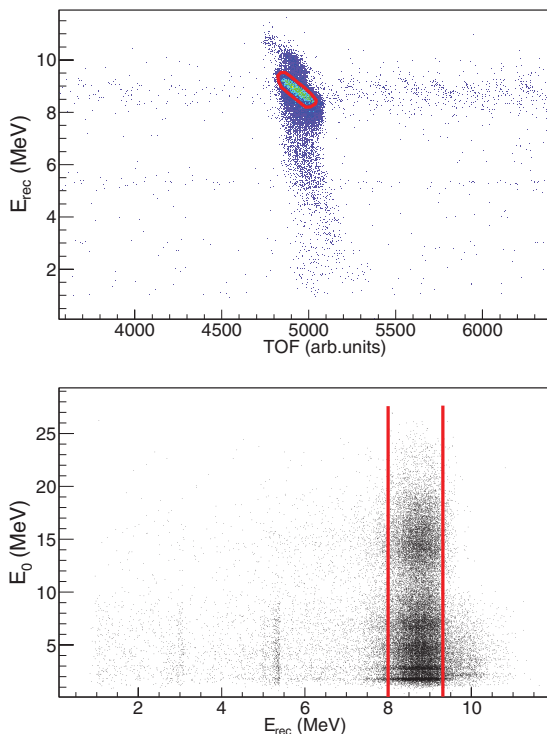


FIG. 4. (Color online) Top: Energy of the recoil nuclei as a function of the TOF between the $\gamma$ ray and the recoil nuclei at $E_{c.m.} = 9$ MeV. Bottom: $E_\gamma$ as a function of the energy of the recoil nuclei; red lines correspond to the region selected.
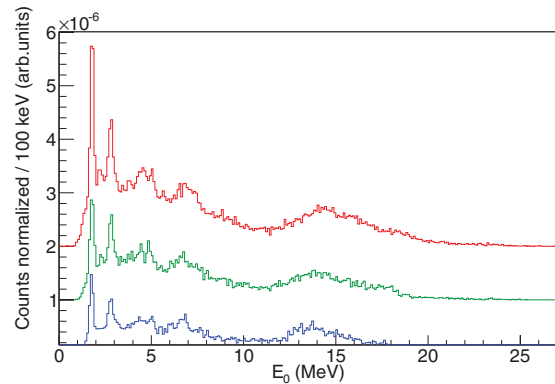


FIG. 5. (Color online) Spectrum of the highest energy $\gamma$-ray $E_0$ in coincidence with the recoil nuclei at the three bombarding energies, corresponding to $E_{c.m.} = 8.5$ MeV (lowest, blue curve), 8.8 MeV (middle, green curve), and 9 MeV (upper, red curve). Each spectrum is normalized to the target thickness and beam charge accumulated.

reflecting the selection of the RC channel. These feedings and particularly the feeding of the $4_1^+$ state are a first indication that there are important contributions of spins $J \geqslant 4\hbar$ in the entrance channel.

### B. Feeding of particular states

The $\gamma$ peak around 7 MeV (see Fig. 5) is in coincidence with $\gamma$ rays up to 18 MeV (Fig. 6) and only weakly with the 1.78-MeV transition. This led us to conclude that we measure there the feeding of the $3^-$ state at 6.88 MeV, which is known to decay mainly to the g.s. In a previous work, the direct feeding of states around 7 MeV has been observed by the detection of high-energy $\gamma$ rays of 18 MeV [17]. This was interpreted by Collins *et al.* in terms of a decay via the $0^+$ and $2^+$ states (at 6.69 and $\sim$7.4 MeV) of the $^{28}$Si prolate band. In the present study, the used experimental setup allowed us to access not only high-energy $\gamma$ rays but also low-energy transitions (down to 1.5 MeV) and thus to show that the dominant feeding was of the $3^-$ state and not of the prolate $0^+$ and $2^+$ states. This $3^-$ state is the first negative-parity state in $^{28}$Si and is the bandhead of the $K^\pi = 3^-$ band. Its quadrupole moment is $|Q_0| \sim 67.5$ $e$ fm$^2$ and its main electromagnetic decay is an accelerated $E3$ transition to the
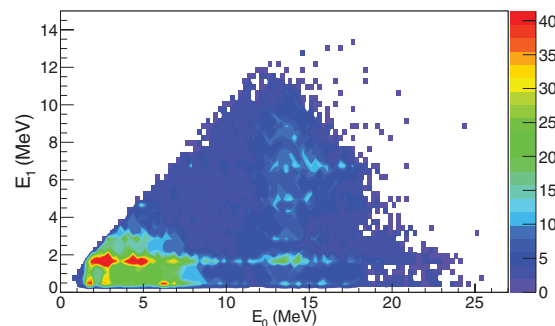


FIG. 6. (Color online) $E_0$, the highest energy $\gamma$ ray measured in a cascade, in coincidence with the recoil nuclei at $E_{c.m.} = 8.5$ MeV, vs $E_1$, the second highest energy $\gamma$ ray.
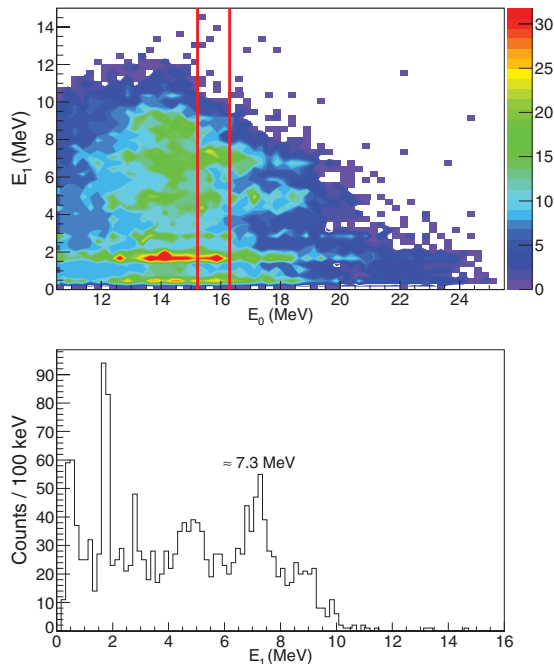
FIG. 7. (Color online) Top: $E_0$ vs $E_1$ at $E_{c.m.} = 9$ MeV. Bottom: $E_1$ spectrum with a gate around 16 MeV on $E_0$ as indicated in the top part.



FIG. 8. (Color online) Experimental angular distribution for the $11 < E_\gamma < 17$ MeV bump region at $E_{c.m.} = 9$ MeV. The red curve corresponds to a fit of the data with a calculated $6^+ \rightarrow 4^+(E2)$ angular distribution.

g.s., with a reduced transition probability $B(E3)$ of 20 W.u. These two characteristics indicate a deformed collective state, which in the literature is discussed in terms of prolate as well as oblate and octupole deformations [18]. At $E_{c.m.} = 9$ MeV, as seen in Fig. 5, a second component rises at the high-energy tail of the 7-MeV peak. It is in coincidence, as shown in Fig. 7, with a $\gamma$ ray of $E_\gamma \sim 16$ MeV and is centered at 7.3 MeV. This peak corresponds to the direct feeding of the $4^+$ state at 9.16 MeV, which is the third member of the known $^{28}$Si prolate band. This band built on the $0_3^+$ satet at 6.69 MeV has a quadrupole moment $Q_0 \sim 87.6e$ fm$^2$ and an axis ratio of 1.52. The energy of this state cannot be reproduced by $0\hbar\omega$ shell-model calculations using the USDB interaction [20]. Multiparticle-hole excitations are probably needed to reproduce this state in terms of shell-model calculations. From the cluster point of view, states with energies close to those of the prolate band are expected with partial $^{12}$C-$^{16}$O structure, as mentioned in the first part of this article.

### C. Angular distribution

The intensity of $\gamma$ rays belonging to the bump at 14 MeV has been normalized by taking into account the response of the detector array to an isotropic distribution. This process enabled us to deduce the corresponding angular distribution. In this $^{12}$C + $^{16}$O experiment, both target and projectile have spin $0^+$ and thus the recoiling $^{28}$Si nuclei produced at $0°$ are aligned and the angular distribution only depends on electromagnetic transition characteristics. The measured angular distribution is presented in Fig. 8 and shows a clear indication of quadrupole ($E2$) electromagnetic transitions.

## IV. DISCUSSION AND INTERPRETATION

### A. Decay scenarios: comparison to GEANT3 simulations

In order to discuss quantitatively the results, it is necessary to take into account how the experimental setup filters the data. As mentioned previously, the DRAGON acceptance and transmission of the recoil nuclei depend on the $\gamma$-decay path. It is thus necessary to unfold the effects of this bias on the $\gamma$ spectra. To achieve this, we have used a GEANT3 code describing the complete DRAGON-BGO apparatus [21,22] and have implemented properties of the recoil nuclei ($A$, $E_{rec}$) and of the $\gamma$ decay of $^{28}$Si*, i.e., full decay path and angular distribution of $E_0$. All aspects of the geometry, the optical elements of DRAGON, and the $\gamma$ detectors have been used to obtain the efficiency of the array for the acceptance and transmission of the recoil nuclei through DRAGON. The experimental resolution of the BGO detectors has been taken into account in the simulated spectra. Our experimental results will be compared with three plausible decay scenarios: a statistical one, a unique entrance spin one, and a cluster one. To allow direct comparison of simulated spectra and experimental data, the total numbers of counts have been normalized to the total numbers of counts in the experimental spectra.

#### 1. Statistical decay

We have used a calculated entrance angular momentum ($L$) distribution as an input of a purely statistical decay. This distribution has been obtained via coupled-channel calculations [23] by taking into account two barriers extracted from a fit to previous fusion data [24,25]. The results are presented in Fig. 9(a) at the three energies of the present study. The $\gamma$ deexcitation for this scenario with no noticeable structure effect will be the basis for further comparison with other decay modes. The branching ratios to the bound or quasibound states of $^{28}$Si [26] have been calculated using the mean electromagnetic transition strengths in the $^{28}$Si mass region reported in the literature [27] by taking into account the self-conjugate character of $^{28}$Si. The angular distribution of the primary decay has been taken into account and the secondary decay characteristics of the considered 69 $^{28}$Si bound or
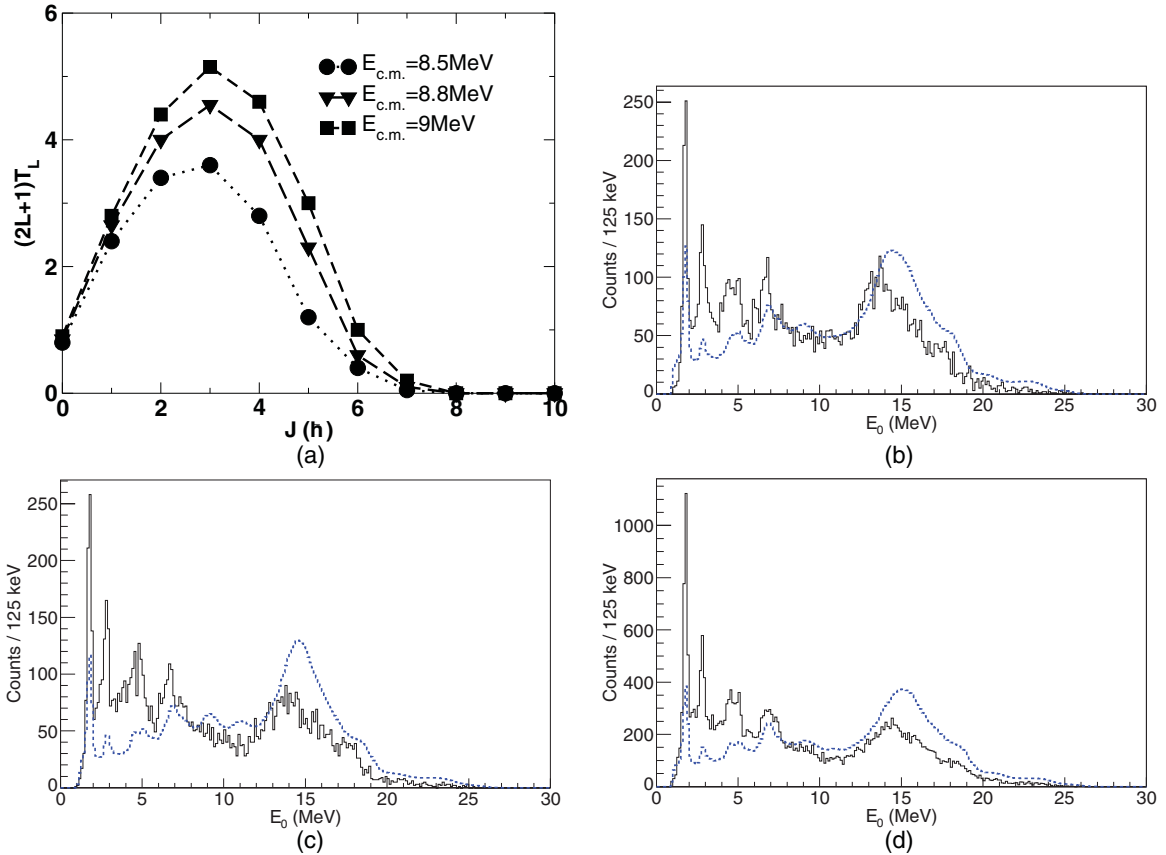
FIG. 9. (Color online) (a) Entrance $L$ distributions obtained by coupled-channel calculations. In our case, the entrance angular momentum $L$ and spin $J$ are the same. $E_0$ spectrum in coincidence with the recoil nuclei (black continuous line) compared to numerical simulations for a pure statistical decay (blue dashed line) at $E_{c.m.} = 8.5$ MeV (b), 8.8 MeV (c), and 9 MeV (d). The $\chi^2$ values per number of degrees of freedom are 11.4, 24.1, and 37.2 at $E_{c.m.} = 8.5$ MeV (b), 8.8 MeV (c), and 9 MeV (d), respectively.

quasibound states have been taken from the literature [26]. The results are presented in Figs. 9(b)–9(d) for the three bombarding energies. The basic statistical decay behavior shows large discrepancies with the experimental data. At all energies, the corresponding $\chi^2$ values per number of degrees of freedom (ndf) is greater than 11. It should be noted that we have identified the specific direct feedings of the $4^+$ and the $3^-$ states and that the statistical entrance spin distribution is mainly centered between $L = 2$ and 4 [see Fig. 9(a)]. This indicates that larger spins than the main statistical ones are certainly needed in the entrance channel to reproduce the data. The second scenario refers to a unique entrance spin decay, meaning that we have considered a nonstatistical behavior instead of a spin distribution in the entrance channel. Such behavior is expected in the case of resonances in the $^{12}C + ^{16}O$ collision. In this scenario, the subsequent $\gamma$ decay has been calculated as previously.

### 2. Unique entrance spin

Figure 10(a) compares experimental data and simulation results for a unique entrance spin between 0 and $8\hbar$ of natural parity. The best reproduction of the experimental data is found for spins $5^-$ and $6^+$, with a deep $\chi^2$ minimum for a $6^+$

entrance state at $E_{c.m.} = 9$ MeV. To mimic a possible statistical background below the unique spin resonance, a fraction of the statistical decay of the precedent scenario has been introduced. We then compare experimental data and simulations with three parameters: the first is the percentage of statistical background; the second and third are the weights (in percent) of the $5^-$ and $6^+$ states, respectively, in the entrance channel. The results are presented in Figs. 10(b)–10(d). At $E_{c.m.} = 8.5$ MeV, good results are obtained for a 44%–56% mixing of $5^-$ and $6^+$ with a $\chi^2$/ndf $\sim$3.7. This should be compared to the value of 11.4 for the basic statistical scenario [see Fig. 9(b)]. In the case of $E_{c.m.} = 8.8$ MeV, the results are not as well reproduced [Fig. 10(c)] and the best $\chi^2$/ndf is 15.6 for a 84%–16% mixing, which is to be compared to $\chi^2$/ndf $\sim$ 24.1 for the statistical decay. Finally, a quasipure $6^+$ resonant behavior, i.e., a 8%–86% mixing, best describes the data at $E_{c.m.} = 9$ MeV with $\chi^2$/ndf $\sim$ 5.6, to be compared to 37.2 for the statistical decay [see Fig. 9(d)].

### 3. Cluster-type decay

The data at $E_{c.m.} = 9$ MeV show a pronounced non-statistical behavior, i.e., the feeding of the $4^+$ state of the prolate band and a clear unique spin $J^\pi = 6^+$ in the
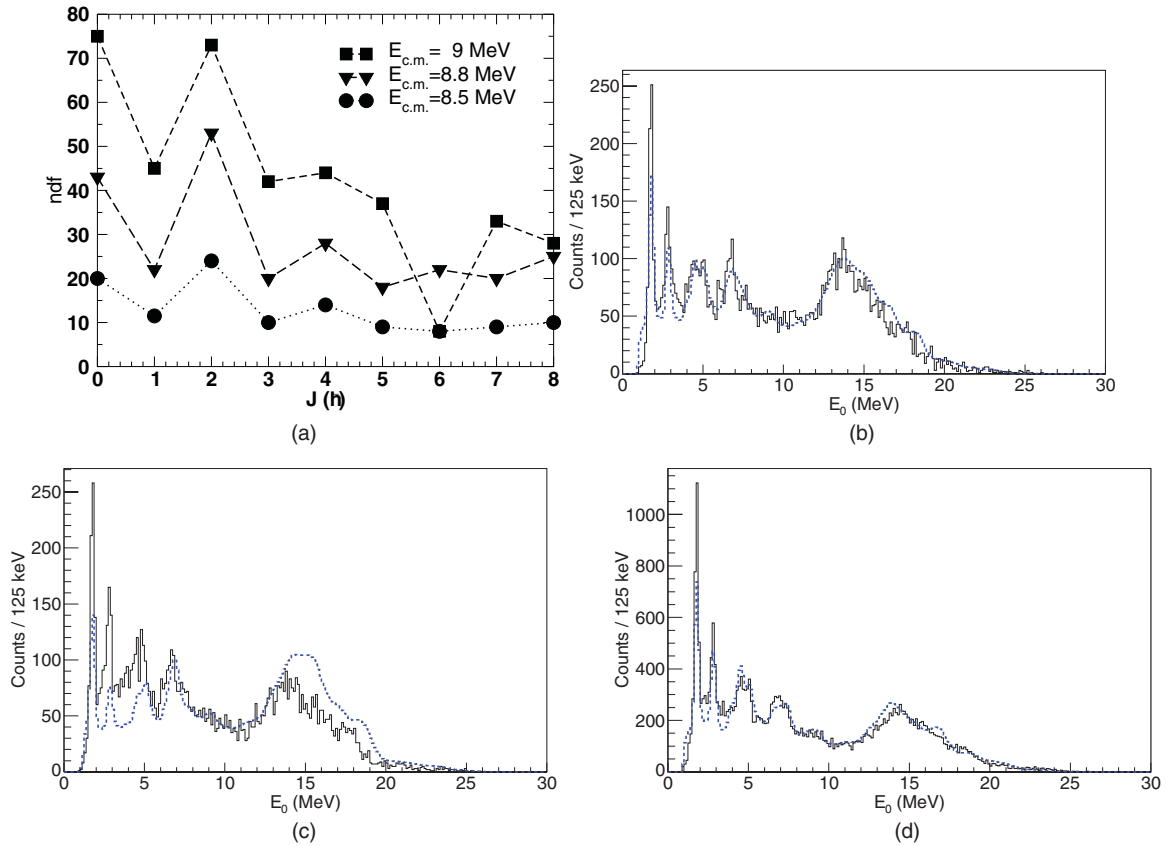
FIG. 10. (Color online) (a) $\chi^2$/ndf simulations for unique different entrance spins $J$ at the three bombarding energies. $E_0$ spectrum in coincidence with the recoil nuclei (black continuous line) compared to numerical simulation for a mixed $5^-/6^+$ spin contribution (blue) at $E_{\text{c.m.}} = 8.5$ MeV (b), 8.8 MeV (c), and 9 MeV (d). The percentage of statistical background is 0% for (b) and (c) and 6% for (d).

entrance channel of the reaction. If the physics behind this behavior consists of molecular states, not only should the spin distribution in the entrance channel be nonstatistical but so should the subsequent $\gamma$ decay as well. To compare our data with a scenario fully based on a cluster model, we have introduced in the simulation the $\gamma$-decay scheme predicted by the semimicroscopic algebraic cluster model [28,29]. In this calculation, the oblate g.s. band is described in terms of $^{24}$Mg $+ \alpha$ substructure, the known prolate band, as well as the resonant band in terms of $^{12}$C $+$ $^{16}$O substructures. The relative strength of transitions between cluster bands has been calculated from the resonant to the prolate band. The transitions between the resonant and the g.s. band cannot be calculated in this way because they do not belong to the same configuration space. The decay characteristics of the intermediate cluster band, which corresponds to the known $^{28}$Si prolate band, have been taken from the literature. As previously explained, a free parameter has been introduced in the calculation for the statistical background. The best result ($\chi^2$/ndf $\sim 9.16$) is obtained with a statistical background of 41%. For a $J^\pi = 6^+$ resonance in the entrance channel, the corresponding spectrum is presented in Fig. 11. The result for the cluster scenario is in better agreement with the data than a fully statistical scenario [$\chi^2$/ndf $\sim 37.2$; see Fig. 9(d)]. Nevertheless, the normal decay of a quasipure $6^+$ entrance state describes best the data [$\chi^2$/ndf $\sim 5.62$; see Fig. 10(d)]. As

seen in Fig. 11, the main differences between the data and the simulation are a lack of flux in the 2.78-MeV peak ($4_1^+ \rightarrow 2_1^+$) and an excess of flux to the $4_3^+$ at 9.16 MeV, which gives rise to too intense a peak around 7 MeV. A better agreement would probably be obtained if a decay from the molecular band to the g.s. band could be incorporated in the cluster model.
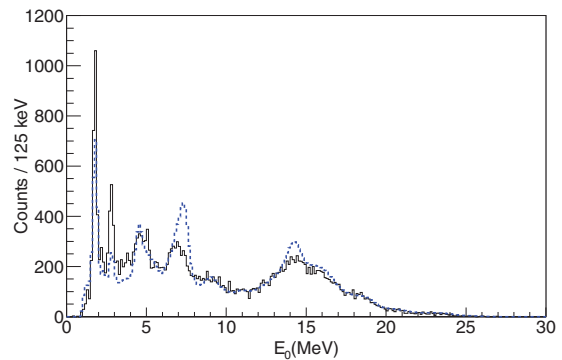


FIG. 11. (Color online) $E_0$ spectrum in coincidence with the recoil nuclei (black continuous line) at $E_{\text{c.m.}} = 9$ MeV compared to numerical simulations (blue dashed line) for the cluster-type decay.

TABLE I. Total and partial RC cross section and distribution of the $\gamma$ flux for the $^{12}$C + $^{16}$O reaction. See text for more details.

| $E_{\text{c.m.}}$(MeV) | 8.5 | 8.8 | 9 |
|---|---|---|---|
| $J^{\pi}$ | $5^-$-$6^+$ | $5^-$-$(6^+)$ | $6^+$ |
| $\sigma_{\text{RC}}$ ($\mu$b) [14,17] | 2.3 | 2 | 3.1 |
| $\sigma_{\text{RC}}$ ($\mu$b) (this measurement) | $11.6 \pm 2.8$ | $16.3 \pm 4.0$ | $23.4 \pm 5.7$ |
| $\sigma_{\text{RC}}$ ($E^* < 5$ MeV) ($\mu$b) | 1.4 | 2.4 | 1.1 |
| $\sigma_{\text{RC}}$ ($5 < E^* < 9$ MeV) ($\mu$b) | 3.2 | 4.3 | 6.9 |
| $\sigma_{\text{RC}}$ ($9 < E^* < 12$ MeV) ($\mu$b) | 7.0 | 9.6 | 15.4 |
| $\sigma_{\text{RC}}/\sigma_{\text{F}}$ ($10^{-5}$) | 6.8 | 7.6 | 9.6 |

## B. Characteristics of the $^{12}$C + $^{16}$O radiative capture reaction

### 1. Cross section

The transmission of the recoil nuclei through DRAGON is an essential ingredient in the comparison of our RC data to simulated decay scenarios to deduce the spins involved in the process but also in extracting the RC cross sections at the three energies of the present study. These cross sections have been obtained by taking into account the $^{28}$Si charge state distribution and in particular the intensity of the charge state $q = 8$ [30]. Results are summarized in Table I, which presents for each energy the proposed entrance spin, the RC cross section in previous work [14,17], and the total RC cross section that we have measured. In this table are also given the partial cross sections corresponding to different excitation energy ($E^*$) regions of $^{28}$Si. Finally, the ratio of the measured RC cross section to the total fusion cross section [24,25] is given in the last line of the table. The main errors on $\sigma_{\text{RC}}$ are due to the systematic uncertainties on the beam charge integration ($\sim$10%), on the thickness of the target ($\sim$10%), and on the transmission of the recoil nuclei ($\sim$20%).

The total RC cross section measured in this experiment is typically seven times larger than previously measured [14,17] due to the fact that in previous experiments the feeding of doorway states with $E^*$ between 9 and 10 MeV could not be measured. From the $\sigma_{\text{RC}}/\sigma_{\text{F}}$ ratios given in Table I as a function of $E_{\text{c.m.}}$, one sees that the capture cross sections show a stronger enhancement than the fusion cross sections. This enhancement as well as the unique entrance spin behavior and the selective feeding of the $4^+$ member of the prolate band favors an interpretation in terms of a nonstatistical process. To get a deeper insight into the reaction mechanisms and their interplay with molecular states, we have performed time-dependent Hartree-Fock (TDHF) calculations, which will be discussed in the next part.

### 2. TDHF description of the $^{12}$C + $^{16}$O collision around the Coulomb barrier

To try to better understand in a dynamical way the presence of resonances and the contribution of relatively large spins at energies close to the CB, we have performed TDHF calculations with a Skyrme interaction using the SLy4d parametrization [31]. The TDHF equation is solved at each time step by the TDHF3D code. The time and lattice steps
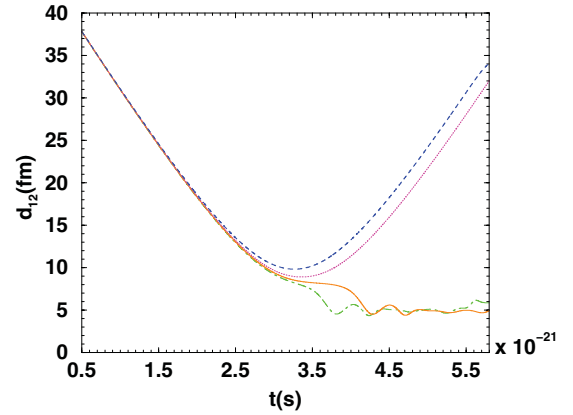


FIG. 12. (Color online) Distance between $^{12}$C and $^{16}$O as a function of time at $E_{\text{c.m.}} = 8.8$ MeV. The different colors correspond to different $\langle L \rangle$: $\langle L \rangle = 3\hbar$ (green dashed-dotted line), 3.9 (orange continuous line), $5\hbar$ (pink dotted line), and $7\hbar$ (blue dashed line).

are $\Delta t = 1.5 \times 10^{-24}$ s and $\Delta x = 0.8$ fm, respectively (see Ref. [32] for more practical details).

We have first estimated the position of the CB by TDHF. To do this, the calculation was done at different bombarding energies to find the critical energy corresponding to the fusion of the two nuclei. A value of $7.8 < $ CB $ < 7.9$ MeV was obtained, in agreement with the coupled-channel calculations mentioned before. In addition, we have also calculated the maximum mean angular momentum $\langle L \rangle$ which allows fusion at the bombarding energies of the present study. As an example, Fig. 12 shows the distance $d_{12}$ between $^{12}$C and $^{16}$O as a function of time for different $\langle L \rangle$. Independently of $\langle L \rangle$, the nuclei will come close to each other up to a time of $3.6 \times 10^{-21}$ s. After this time, the system fuses or scatters depending on $\langle L \rangle$. Critical mean angular momentum $\langle L \rangle_{\text{critical}}$ values corresponding to the fusion regime are 3.2, 3.9, and 4.4 for $E_{\text{c.m.}} = 8.5$, 8.8, and 9 MeV, respectively. At these energies, the corresponding TDHF fusion cross sections are 151, 208, and 253 mb, respectively. This is in good agreement with the experimental fusion cross-section values, which are 171, 215, and 244 mb for $E_{\text{c.m.}} = 8.5$, 8.8, and 9 MeV, respectively [22,24,25]. The $\langle L \rangle_{\text{critical}}$ values are smaller than the dominant spins $5\hbar$ and $6\hbar$ measured at these energies. This indicates that these spins are populated by a direct transition toward resonant states of the compound nucleus. It is worth mentioning that the estimated grazing angular momentum $\langle L \rangle_{\text{grazing}}$ values at our three bombarding energies, calculated semiclassically, are 3.9, 4.7, and 5.2, i.e., larger by $\Delta L \sim 0.8$ than $\langle L \rangle_{\text{critical}}$, and also closer to the experimentally determined spin values.

In the fusion mechanism, the system spends some time in a dinuclear configuration, which presents some analogies with a molecular state. The excitation of the latter is then expected to increase with the lifetime of the dinuclear system. The definition chosen in TDHF for the existence of a dinucleus is the following: the nuclear density at the neck should be between 0.004 and 0.14 fm$^{-3}$, i.e., lower than the saturation density of 0.16 fm$^{-3}$. These nuclear densities correspond to distances between $^{12}$C and $^{16}$O from 5.98 to 10.43 fm. The dinuclear lifetime is shown as a function of
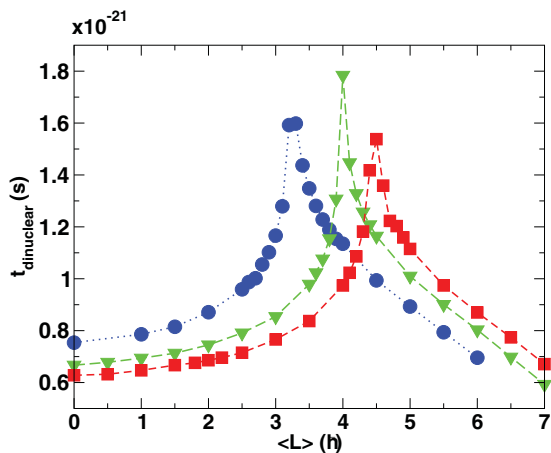
FIG. 13. (Color online) Dinuclear lifetimes $t_{dinuclear}$ as a function of the mean angular momentum $\langle L \rangle$ at $E_{c.m.} = 8.5$ MeV (blue circles), 8.8 MeV (green triangles), and 9 MeV (red squares).

$\langle L \rangle$ in Fig. 13. Below $\langle L \rangle_{critical}$, this time increases with $\langle L \rangle$ because the fusion process is slowed down by the centrifugal repulsion. In contrast, for $\langle L \rangle$ greater than $\langle L \rangle_{critical}$, the fragments reseparate and the time of contact decreases for more peripheral collisions. With the present definition of the dinuclear system lifetime, we see that such a system exists at angular momenta of $5\hbar$ and $6\hbar$. The corresponding lifetimes are shorter than the lifetimes of typical resonances at the CB, which are $\sim 2.6 \times 10^{-21}$ s [7,8]. However, it may be sufficient to allow a direct excitation of a resonant or molecular state of the compound nucleus with a similar structure. In particular, we see that, for $\langle L \rangle = 5\hbar$ and $6\hbar$ (above the critical angular momenta), the lifetime increases with energy. Similarly, the probability for the population of a molecular state is also expected to increase. This may explain why the cross section for radiative capture increases with energy for these spins.

## V. CONCLUSION AND PERSPECTIVES

For the first time, the complete decay of the RC reaction $^{12}$C($^{16}$O,$\gamma$)$^{28}$Si and the relative strengths of all decay pathways have been measured at three energies close to the CB: $E_{c.m.} = 8.5$, 8.8, and 9 MeV. The results obtained show in particular that 70% of the $\gamma$ flux feeds quasibound states around 11 MeV in $^{28}$Si* and that the $3^-$ ($E^* = 6.88$ MeV) and $4^+$ ($E^* = 9.16$ MeV) deformed states are selectively populated. The RC mechanism allows us to probe both the entrance channel by its overlap with the states of the composite nuclei and the

nature of the states fed via electromagnetic transitions. In order to discuss the statistical versus the structural aspect of the entrance channel and of the $\gamma$ decay, the data have been compared with three scenarios: a pure statistical one, a resonant one with a single entrance channel spin, and one based on a cluster description of $^{28}$Si. For the three energies studied, a pure statistical behavior is clearly unable to describe the $\gamma$ spectra recorded. In particular, higher spins ($5\hbar$ and $6\hbar$) are needed to reproduce the $\gamma$ spectra. This nonstatistical behavior is stronger at $E_{c.m.} = 9$ MeV and, in particular, the selective feeding of the $4^+$ state of the prolate band is a good indication of the occurrence of a $\gamma$ transition between molecular bands. These higher spins are in good agreement with the fusion resonance work [7,9], where tentative spins of $4^+$, $5^-$, and $6^+$ are proposed in the energy range between 8.45 and 9.26 MeV, i.e., in a region covered in the present work. Comparisons with Monte Carlo simulations of the experimental setup and of the complete $^{28}$Si decay scheme have allowed us to extract full RC cross sections which are much larger than those previously known due to the observation in our work of the feeding of "doorway" states. As seen in Table I, this feeding is much larger than that of the low-lying states. The RC cross sections range from 12 to 25 $\mu$b, greatly in excess of the usual values for such cross sections ($\sim$500 nb [14]) close to the CB. TDHF calculations have been performed to understand the role of angular momentum in the entrance channel and the formation of a dinucleus in the process. All these results in the $^{28}$Si nuclei in which prolate, oblate, and octupolar shapes coexist at relatively low excitation energy point out how deformation influences the RC process. Unfortunately, a complete energy identification of the $\gamma$ spectra is hampered by the poor resolution of the BGO scintillators. This has prevented us from further specifying the nature and number of states fed around 11 MeV in $^{28}$Si. In a near future, this lack of resolution could be overcome with the development of a new kind of scintillator such as LaBr$_3$. Numerical simulations for the future PARIS detector, based on this type of crystal [33], show that the resolution and efficiency achieved [34,35] will permit us to disentangle the different scenarios proposed in this work.

[1] W. von Oertzen, M. Freer, and Y. Kanada-En'yo, Phys. Rep. **432**, 43 (2006), and references therein.

[2] Y. Kanada-En'yo, M. Kimura, and H. Horiuchi, Nucl. Phys. A **738**, 3 (2004).

[3] Y. Taniguchi, Y. Kanada-Enyo, and M. Kimura, Phys. Rev. C **80**, 044316 (2009).

[4] Y. Taniguchi, M. Kimura, Y. Kanada-En'Yo, and H. Horiuchi, Int. J. Mod. Phys. E **20**, 1046 (2011).

[5] T. Ichikawa, Y. Kanada-En'yo, and P. Möller, Phys. Rev. C **83**, 054319 (2011), and references therein.

[6] J. Cseh, Phys. Rev. C **50**, 2240 (1994).

[7] E. C. Schloemer *et al.*, Phys. Rev. Lett. **51**, 881 (1983).

[8] K. A. Erb and D. A. Bromley, *Treatise on Heavy Ion Science*, edited by A. Bromley (Plenum, New York, 1985), Vol. 3, p. 201, and references therein.

[9] W. Treu *et al.*, Phys. Lett. B **72**, 315 (1978).

[10] C. J. Metelko *et al.*, J. Phys. G **29**, 697 (2003).

[11] T. Spillane *et al.*, Phys. Rev. Lett. **98**, 122501 (2007).

[12] Y. Suzuki and K. T. Hecht, Nucl. Phys. A **388**, 102 (1982).

[13] J. Cseh, G. Lévai, and W. Scheid, Phys. Rev. C **48**, 1724 (1993).

[14] A. M. Sandorfi, *Treatise on Heavy Ion Science*, edited by A. Bromley (Plenum, New York, 1984), Vol. 2, p. 53, and references therein.

[15] D. G. Jenkins *et al.*, Phys. Rev. C **71**, 041301(R) (2005).

[16] D. G. Jenkins *et al.*, Phys. Rev. C **76**, 044310 (2007).

[17] M. T. Collins, A. M. Sandorfi, D. H. Hoffmann, and M. K. Salomaa, Phys. Rev. Lett. **49**, 1553 (1982).

[18] R. K. Sheline, S. Kubono, K. Morita, and M. H. Tanaka, Phys. Lett. B **119**, 263 (1982).

[19] D. A. Hutcheon *et al.*, Nucl. Instrum. Methods A **498**, 190 (2003).

[20] B. A. Brown and W. A. Richter, Phys. Rev. C **74**, 034315 (2006).

[21] J. Slater, Internal Report of the DRAGON-TRIUMF group, May 2004.

[22] D. Lebhertz, PhD. thesis, University of Strasbourg, 2009.

[23] K. Hagino, N. Rowley, and A. T. Kruppa, Comput. Phys. Commun. **123**, 143 (1999).

[24] P. R. Christensen, Z. E. Switkowski, and R. A. Dayras, Nucl. Phys. A **280**, 189 (1977).

[25] B. Cujec and C. A. Barnes, Nucl. Phys. A **266**, 461 (1976).

[26] http://www.nndc.bnl.gov/nudat2/ and the adopted levels therein.

[27] P. M. Endt, At. Data Nucl. Data Tables **55**, 171 (1993).

[28] J. Cseh, Phys. Rev. C **50**, 2240 (1994).

[29] J. Cseh and G. Lévai, Ann. Phys. (NY) **230**, 165 (1994).

[30] K. Shima, N. Kuno, M. Yamanouchi, and H. Tawara, At. Data Nucl. Data Tables **51**, 173 (1992).

[31] K.-H. Kim, T. Otsuka, and P. Bonche, J. Phys. G **23**, 1267 (1997).

[32] C. Simenel, D. Lacroix, and B. Avez, *Quantum Many Body Dynamics: Applications to Nuclear Reactions* (VDM Verlag, Sarrebruck, Germany, 2010).

[33] A. Maj *et al.*, Acta Phys. Pol. B **40**, 565 (2009).

[34] D. Lebhertz *et al.*, Int. J. Mod. Phys. E **20**, 793 (2011).

[35] D. Lebhertz *et al.*, Acta Phys. Pol. B **42**, 721 (2011).